

# Landau-Khalatnikov Circuit model for Ferroelectric Hysteresis

S. Sivasubramanian and A. Widom

*Physics Department, Northeastern University, Boston MA 02115*

(Dated: October 22, 2018)

We present the circuit equivalent of the Landau-Khalatnikov dynamical ferroelectric model. The differential equation for hysteretic behavior is subject to numerical computer simulations. The size and shape of the simulated hysteretic loops depends strongly on the frequency and the amplitude of the driving electric field. This dependence makes the experimental extraction of the coercive electric field difficult. The bifurcation of the driven Landau-Khalatnikov model is explained in detail.

PACS numbers: 77.80.Dj, 77.80.Fm, 77.22.Gm

## I. INTRODUCTION

Many of the interesting properties of ferroelectric materials are probed experimentally by measuring the polarization response to a time varying electric field. These properties form the basis for important potential computer engineering applications[1, 2, 3, 4] such as ferroelectric random access memory or ferroelectric memory field effect transistors. A common method to observe ferroelectric polarization features is via the hysteresis loop. A sinusoidal electric field is applied to the ferroelectric sample while the polarization  $\mathbf{P}$  and/or polarization current density  $\mathbf{J} = (\partial\mathbf{P}/\partial t)$  is continuously monitored. The observed data is then in principle utilized to determine the thermal remnant polarization  $\mathbf{P}_s$  and coercive field  $\mathbf{E}_c$ .

Some of the partially understood experimental results are as follows: (i) No unique coercive field is evident during the hysteretic process of switching. (ii) When an alternating electric field is applied, a hysteretic loop is observed only within a limited frequency band and a limited range of amplitudes. (iii) Multiple hysteresis loops are commonly observed.

Various approaches have been adopted to explain these strange characteristic features of the ferroelectric materials. One approach is to create a equivalent circuit models[5, 6, 7, 8, 9, 10, 11, 12, 13] that simulate the experimental data. The earliest among these models are the Sawyer-Tower circuit[14] and modifications thereof[15, 16] which are used to study the hysteretic properties of ferroelectric capacitors. Currently, many of the circuit models are computed using the SPICE[17] simulations. Previous circuit models depend strongly upon which particular applications one is interested in analyzing. No single standard circuit has been put forward to explain the great variety of experimental results available for different regimes of electric field and frequency. Our goal is to explore many of the experimentally observed properties employing a single circuit model. The model is equivalent to the Landau-Khalatnikov dynamical equation for the ferroelectric polarization. This non-linear circuit model produces a variety of previously unexpected hysteretic behaviors.

In Sec. II we present the circuit equivalent of the

Landau-Khalatnikov[18, 19, 20, 21] dynamical ferroelectric model. In Sec. III the differential equations which must be solved are written in the “dimensionless” form suitable for numerical simulations. In Sec. IV the dependence of the size and shape of the simulated hysteretic loops on the frequency and amplitude of the driving electric field will be exhibited. Sec. V deals with the bifurcation of hysteretic curves. The dynamical properties of the model contains a regime of broken symmetry and a regime of unbroken symmetry. The conventional hysteretic loops are in the symmetric dynamical regime. In the concluding Sec. VI future experimental prospects for the model are explored.

## II. THE LANDAU-KHALATNIKOV CIRCUIT

The thermodynamic equations of state for a ferroelectric model are described by the energy per unit volume  $U(\mathbf{P}, S)$  as a function of polarization and entropy per unit volume obeying

$$dU = \mathbf{E}_{thermal} \cdot d\mathbf{P} + TdS. \quad (1)$$

In addition to the thermal electric field, a ferroelectric sample exhibits a dissipative electric field derived from an Ohm’s law resistivity  $\rho$ ,

$$\mathbf{E}_{Ohm} = \rho\mathbf{J} = \rho \left( \frac{\partial\mathbf{P}}{\partial t} \right). \quad (2)$$

The total electric field  $\mathbf{E} = \mathbf{E}_{thermal} + \mathbf{E}_{Ohm}$  gives rise to the Landau-Khalatnikov dynamical equation of motion

$$\mathbf{E} = \left( \frac{\partial U}{\partial \mathbf{P}} \right)_S + \rho \left( \frac{d\mathbf{P}}{dt} \right). \quad (3)$$

Finally, the Maxwell displacement field  $\mathbf{D}$  within a ferroelectric material is given by

$$\mathbf{D} = \epsilon_0\mathbf{E} + \mathbf{P}. \quad (4)$$

If the ferroelectric material is placed inside of a capacitor, then the total charge on one capacitor electrode is given by the surface integral

$$Q_{tot} = \oint_{electrode} \mathbf{D} \cdot d\Sigma. \quad (5)$$

Were the capacitor electrodes embedded in the vacuum, then the capacitor charge would be

$$\mathcal{Q}_{vac} = \epsilon_0 \oint_{electrode} \mathbf{E} \cdot d\Sigma. \quad (6)$$

In general, Eqs.(4), (5) and (6) imply

$$\mathcal{Q}_{tot} = \mathcal{Q}_{vac} + \mathcal{Q} \quad (7)$$

where

$$\mathcal{Q} = \oint_{electrode} \mathbf{P} \cdot d\Sigma. \quad (8)$$

Eq.(7) describes the charges on two capacitors in parallel with the geometrical capacitance  $C_0$  relates the charge to voltage ratio of the vacuum

$$\mathcal{Q}_{vac} = C_0 V. \quad (9)$$

Eqs.(3) and (8) describe the Landau-Khalatnikov dynamics for the non-linear capacitor in FIG. 1 with voltage  $\mathcal{V}(\mathcal{Q})$  connected in series with an Ohm's law resistor  $R$ ; i.e.

$$V = \mathcal{V}(\mathcal{Q}) + R \left( \frac{d\mathcal{Q}}{dt} \right). \quad (10)$$

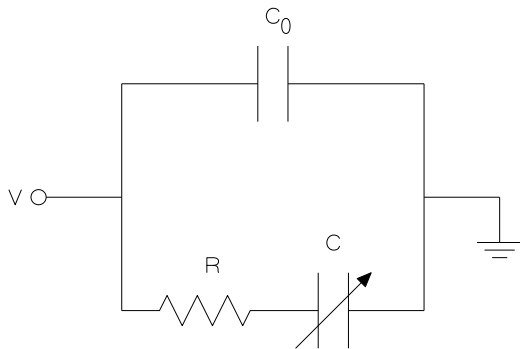


FIG. 1: The equivalent circuit to the Landau-Khalatnikov dynamical equation is shown in the above figure. The linear capacitor is on the upper branch of the circuit and the non-linear capacitor is on the lower branch. The polarization energy  $\mathcal{U}$  is stored in the non-linear capacitor. The ohmic resistor  $R$  describes the dissipation due to time variations in the ferroelectric polarization. The geometric capacitance  $C_0$  is defined in Eq.(9).  $V$  is the applied voltage across the parallel circuit.

If  $\mathcal{U}(\mathcal{Q}, \mathcal{S})$  denotes the energy of the non-linear capacitance, then

$$d\mathcal{U} = Td\mathcal{S} + \mathcal{V}d\mathcal{Q}. \quad (11)$$

The circuit version of Eq.(3) is that

$$V = \left( \frac{\partial \mathcal{U}}{\partial \mathcal{Q}} \right)_S + R \left( \frac{d\mathcal{Q}}{dt} \right). \quad (12)$$

The circuit Eq.(12) is pictured in FIG. 1. In the Landau-Khalatnikov circuit, the upper capacitor carries a charge  $\mathcal{Q}_{vac} = C_0 V$  while the lower non-linear capacitor carries a charge  $\mathcal{Q}$  and voltage  $\mathcal{V}$  determined by the thermodynamic Eq.(11). The resistance  $R$  describes the dissipation present when the polarization varies with time.

### III. PERIODIC VOLTAGE SOURCES

Hysteretic cycles are measured applying a time varying voltage of the form

$$V(t) = V_0 \cos(\omega t). \quad (13)$$

For the case of the Landau energy shown in FIG. 2,

$$\mathcal{U}(\mathcal{Q}) = \left( \frac{\mathcal{Q}_s^2}{8C} \right) \left( 1 - \left( \frac{\mathcal{Q}}{\mathcal{Q}_s} \right)^2 \right)^2, \quad (14)$$

where the saturation polarization  $\mathbf{P}_s$  determines

$$\mathcal{Q}_s = \oint_{electrode} \mathbf{P}_s \cdot d\Sigma, \quad (15)$$

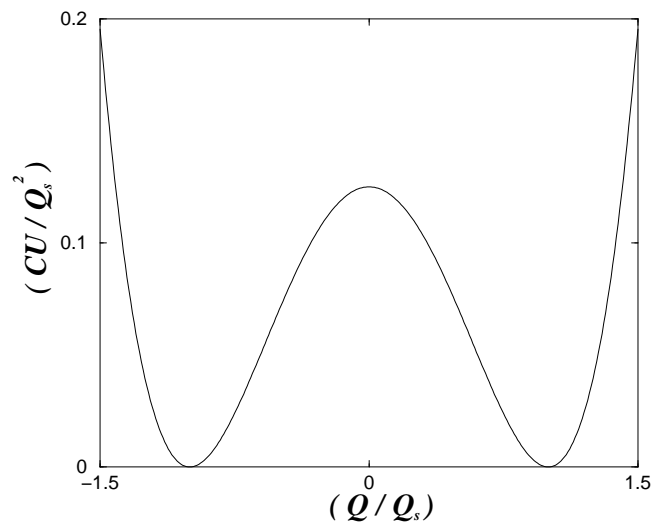


FIG. 2: Shown is the Landau energy for a ferroelectric model. The energy stored in the non-linear capacitor is given by  $U = (Q_s^2/8C)\{1 - (Q/Q_s)^2\}^2$ .

Eqs.(12), (13) and (14) read

$$R \left( \frac{dQ}{dt} \right) + \left( \frac{Q}{2C} \right) \left\{ \left( \frac{Q}{Q_s} \right)^2 - 1 \right\} = V_0 \cos(\omega t). \quad (16)$$

In order to solve Eq.(16) numerically, let us introduce the dimensionless quantities

$$\theta = \omega t, \quad y = (Q/Q_s), \quad \eta = (2\omega RC)^{-1}$$

and

$$z = (V_0/R\omega Q_s). \quad (17)$$

Eqs.(16) and (17) now read

$$\left( \frac{dy}{d\theta} \right) + \eta y(y^2 - 1) = z \cos \theta \quad (18)$$

One seeks solutions to Eq.(18) which are periodic

$$y(\theta + 2\pi; z, \eta) = y(\theta; z, \eta). \quad (19)$$

For example, let us suppose that at an initial time zero

$$y(\theta = 0; z, \eta) = x. \quad (20)$$

After a numerical integration through one period of motion, one then finds that

$$y(\theta = 2\pi; z, \eta) = \mathcal{G}(x; z, \eta). \quad (21)$$

Eqs.(18), (20) and (21) define the function  $\mathcal{G}(x; z, \eta)$ . It is possible to analytically compute  $\mathcal{G}(x; z, \eta)$  in two limits:

$$\lim_{\eta \rightarrow 0} \mathcal{G}(x; z, \eta) = x, \quad (22)$$

$$\lim_{z \rightarrow 0} \mathcal{G}(x; z, \eta) = \left( \frac{x \exp(2\pi\eta)}{\sqrt{1 + x^2(\exp(4\pi\eta) - 1)}} \right). \quad (23)$$

A sufficient condition for existence of periodic Eq.(19) solutions of Eq.(18) is that  $x$  be a fixed point (solution) of the equation

$$x = \mathcal{G}(x; z, \eta). \quad (24)$$

If Eq.(24) has a unique solution for  $x$ , then there exists a unique periodic solution of Eq.(18). If Eq.(24) had more than one solution for  $x$ , then there will be (in general) more than one periodic solution to Eq.(18). The number of solutions for  $x$  depends on the values of parameters in the  $(z, \eta)$  plane.

#### IV. HYSTERESIS CURVES

In this section we consider the region in the  $(z, \eta)$  plane for which the following conditions hold true: (i) Eq.(24) has a unique solution for  $x$  and (ii) there there exists a

unique periodic solution for  $y(\theta; z, \eta)$ . A hysteretic loop located in the  $(Q, V)$  plane may be found by eliminating the time parameter  $t$  in a one period interval  $0 \leq t \leq (2\pi/\omega)$  from the parametric equations

$$Q = Q_s y(\theta = \omega t; z, \eta) \quad \text{and} \quad V = R\omega Q_s z \cos(\omega t). \quad (25)$$

In FIG. 3, we have plotted two hysteretic loops corresponding to the same frequency but with different driving voltage amplitudes. The inner smaller hysteretic loop corresponds to a smaller driving voltage than that of the outer larger hysteretic loop. In FIG. 4 we have plotted two hysteretic loops corresponding to the same voltage amplitude but with different frequencies. The inner smaller hysteretic loop corresponds to a lower frequency than that of the outer larger hysteretic loop.

Since the large amplitude and high frequency loops have a larger enclosed area than do the small amplitude and low frequency loops, it is not at once evident how to extract the coercive voltage directly from hysteretic loop data. This is a well known problem in attempting to measure the coercive electric field forcing a polarization flip. The nature of the problem becomes evident from a study of the effective circuit in FIG. 1. The *theoretical* “coercive voltage”  $\mathcal{V}_c$  is that voltage across the lower branch non-linear capacitor present at the time when the polarization flips. The *experimental* “coercive voltage”  $V_c^{(exp)} = RI_c + \mathcal{V}_c$  includes the voltage across the resistor. It is not an easy matter to separate the dissipative voltage from the thermal capacitor voltage.

In order to understand the “area” enclosed by the hysteresis loop in the  $(Q, V)$  plane, one notes that the ther-

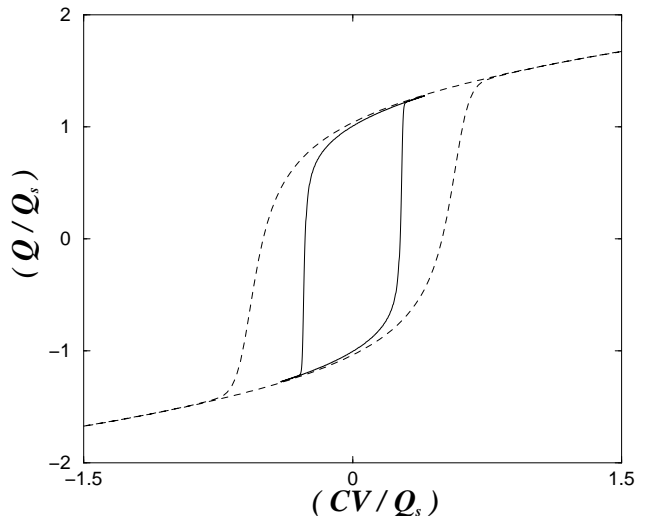


FIG. 3: Shown are two different hysteretic loops simulated for identical frequencies but differing amplitudes of the applied voltage. The smaller inner hysteretic loop corresponds to  $z = 20.0$  and  $\eta = 25.0$ . The larger outer hysteretic loop corresponds to  $z = 200.0$  and  $\eta = 25.0$ . Large applied amplitudes imply high apparent values for the experimental coercive voltages.

modynamic work performed by the non-linear capacitor during one cycle is given by

$$-W(\text{cycle}) = \oint_{\text{loop}} V d\mathcal{Q}, \quad (26)$$

which is also (via the first law of thermodynamics) the heat dissipated by the resistor  $R$  during the cycle. The area enclosed by the hysteretic loop is large or small, respectively, when the dissipated heat in the resistor is large or small.

In order to understand the role of dissipative heating in more detail, multiply Eq.(10) by the current

$$I = \left( \frac{d\mathcal{Q}}{dt} \right) \quad (27)$$

and integrate the result over time for one cycle; i.e.

$$\oint_{\text{loop}} V I dt = \oint_{\text{loop}} \left( \frac{d\mathcal{U}}{d\mathcal{Q}} \right) \left( \frac{d\mathcal{Q}}{dt} \right) dt + \oint_{\text{loop}} R I^2 dt. \quad (28)$$

The first term on the right hand side of Eq.(28) obeys

$$\oint_{\text{loop}} d\mathcal{U} = 0. \quad (29)$$

We then see directly that the work done by the non-linear capacitor during one cycle must be dissipated as heat in the resistor; i.e. Eqs.(26), (27), (28) and (29) imply

$$-W(\text{cycle}) = \oint_{\text{loop}} V I dt = \oint_{\text{loop}} R I^2 dt. \quad (30)$$

Thus, a large applied voltage amplitude and/or a large applied voltage frequency yield a large area loop because more heat is dissipated per cycle by the resistor.

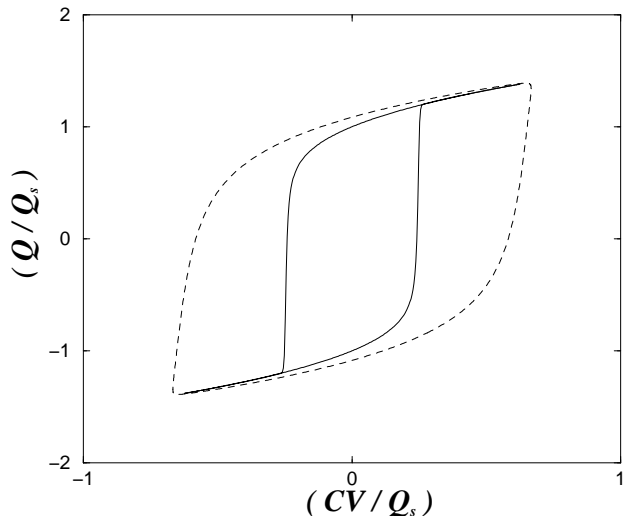


FIG. 4: Shown are two different hysteretic loops simulated for identical amplitudes but differing frequencies of the applied voltage. The smaller inner hysteretic loop corresponds to  $z = 100.0$  and  $\eta = 80.0$ . The larger outer hysteretic loop corresponds to  $z = 3.0$  and  $\eta = 2.25$ . Large applied frequencies imply high apparent values for the experimental coercive voltages.

## V. DYNAMICAL BROKEN SYMMETRY

From the parity symmetry of the energy equation of state  $\mathcal{U}(-\mathcal{Q}, \mathcal{S}) = \mathcal{U}(\mathcal{Q}, \mathcal{S})$ , there are two possible thermal equilibrium minimum energy states at  $\mathcal{Q}_{\pm} = \pm \mathcal{Q}_s$  in the absence of a driving voltage. For a *small driving amplitude*  $V_0$  in Eq.(13), we then expect two possible periodic charge response functions  $\mathcal{Q}_{\pm}(t + (2\pi/\omega)) = \mathcal{Q}_{\pm}(t)$ ;

$$\mathcal{Q}_+(t) \neq \mathcal{Q}_-(t) \implies \text{Broken Symmetry} . \quad (31)$$

On the other hand, for a *large driving amplitude*  $V_0$  in Eq.(13), we expect a unique periodic charge response functions  $\mathcal{Q}(t + (2\pi/\omega)) = \mathcal{Q}(t)$ ;

$$\mathcal{Q}_+(t) = \mathcal{Q}_-(t) \implies \text{Restored Symmetry} . \quad (32)$$

In terms of the dimensionless variables in Eq.(17),

$$z = V_0/(R\omega\mathcal{Q}_s) \quad \text{and} \quad \eta = 1/(2\omega RC), \quad (33)$$

one expects the two regimes to be described by a dynamical bifurcation function  $B(\eta)$

$$z < B(\eta) \implies \text{Broken Symmetry} , \quad (34)$$

$$z > B(\eta) \implies \text{Restored Symmetry} . \quad (35)$$

We have numerically computed  $B(\eta)$  and the results are plotted in FIG. 5. The regions in the  $(z, \eta)$  plane are exhibited corresponding to the symmetric and broken symmetry dynamical phases. In the broken symmetry phase, there are two possible hysteretic curves;  $\mathcal{Q}_+(t)$  is localized in the neighborhood of  $+\mathcal{Q}_s$  and  $\mathcal{Q}_-(t)$  is localized in the neighborhood of  $-\mathcal{Q}_s$ .

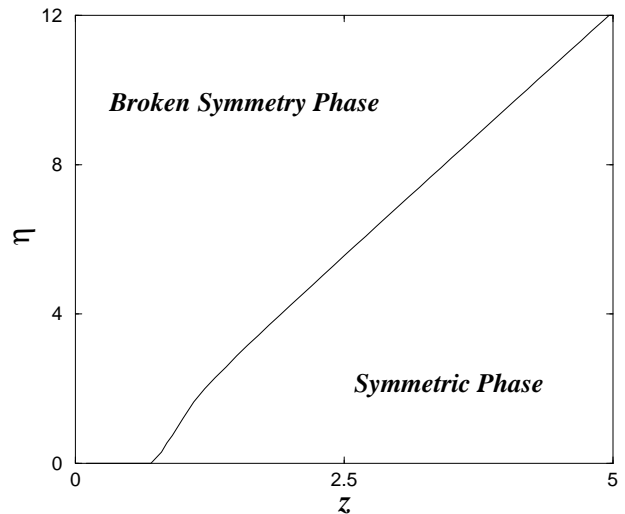


FIG. 5: Shown is the phase plane for the Landau-Khalatnikov model with the dynamical bifurcation curve  $z = B(\eta)$ . If  $z < B(\eta)$ , then parity symmetry is broken. If  $z > B(\eta)$ , then the parity symmetry is restored.

For a more clear picture of the bifurcation[22, 23, 24] boundary curve at  $z = B(\eta)$  we show a sequence of hysteretic loops in FIG. 6. For  $\eta = 0.10$ , we have chosen four values for the amplitudes  $z$ . Explicitly

$$0 < z_a = 0.1 < z_b = 0.7 < B(\eta = 0.1)$$

for illustrations of broken symmetry, and

$$B(\eta = 0.1) < z_c = 1.0 < z_d = 20.0$$

for illustrations of unbroken symmetry. The two ovals in both FIG. 6(a) and FIG. 6(b) correspond, respectively, to  $Q_{\pm}(t)$  for the values  $z_a$  and  $z_b$ . The symmetry is broken because only *one* of the ovals ( $Q_+$  or  $Q_-$  but not both) will appear in an experiment described by the model. The oval in the unbroken symmetry phase corresponding to  $z_c$  is unique but does not appear very similar to conventional hysteretic curves. By increasing the amplitude to  $z_d > z_c$  a conventional looking hysteretic loop appears in FIG. 6(d).

## VI. CONCLUSIONS

It has been shown that the Landau-Khalatnikov model of ferroelectric hysteresis has a very rich dynamical structure. Only a small part of the symmetric dynamical phase had been reported in standard literature. The conventional looking hysteretic curves are present theoretically and experimentally only in the regime of high

driving amplitudes. The region in the neighborhood of the bifurcation into the broken symmetry phase has received little or no experimental attention. The numerical simulations of this work indicate what is to be expected. Experimental measurements of the dynamical bifurcation curve  $z = B(\eta)$  of ferroelectrics would be of great interest in checking the validity of the Landau-Khalatnikov model.

Further insights on how to measure the coercive voltage can be obtained by driving the circuit in FIG. 1 with a voltage source which has both DC and AC components

$$V(t) = V_{ext} + V_1 \cos(\omega t). \quad (36)$$

The DC voltage component  $V_{ext}$  can be put into the energy function via

$$\mathcal{U}(Q, S) \rightarrow \mathcal{U}(Q, S; V_{ext}) = \mathcal{U}(Q, S) - V_{ext}Q, \quad (37)$$

leaving Eq.(12) in the form

$$V_0 \cos(\omega t) = \left( \frac{\partial \mathcal{U}(Q, S; V_{ext})}{\partial Q} \right) + R \left( \frac{dQ}{dt} \right). \quad (38)$$

The advantage of employing a DC component is now evident. The symmetry breaking of the energy in FIG. 2 will now be controlled by varying the DC voltage. The DC offset will allow for precise measurements of the coercive field.

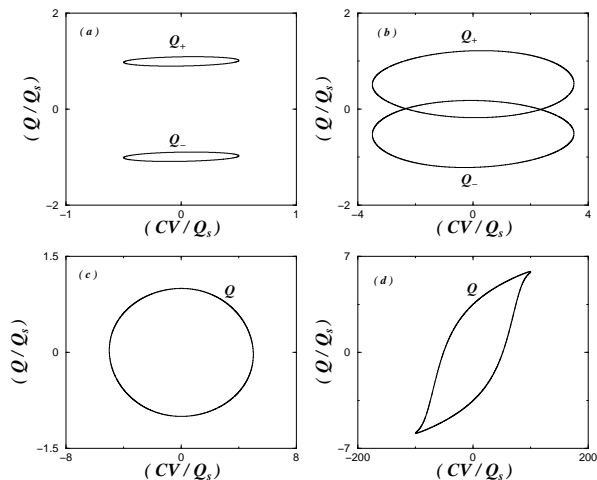


FIG. 6: Shown are four loop plots choosing  $\eta = 0.1$ . (a) For the small amplitude  $B(\eta = 0.1) > z_a = 0.1$ , there are two possible small oval loops. Only one will be realized in a particular experiment. (b) As the voltage amplitude is increased to  $B(\eta = 0.1) > z_b = 0.7 > z_a$  the ovals grow large but are still representative of two different loops. (c) In the symmetric phase  $z_c = 1.0 > B(\eta = 0.1)$ , only a single loop is allowed which does not yet look very close to conventional hysteretic loops. (d) For large voltage amplitude  $z_d = 20.0 > z_c > B(\eta = 0.1)$ , the conventional hysteretic loop is recovered for the model.

- 
- [1] MRS Bull. **21**, 7 (1996).
- [2] M. W. J. Prins, K.-O. Grosse-Holz, G. Müller, J. F. M. Cillessen, J. B. Giesbers, R. P. Weening and R. M. Wolf *Appl. Phys. Lett.* **68**, 3650 (1996).
- [3] M. W. J. Prins, S. E. Zinnemers, J. F. M. Cillessen and J. B. Giesbers, *Appl. Phys. Lett.* **70**, 458 (1997).
- [4] Y. T. Kim and D. S. Shin, *Appl. Phys. Lett.* **71**, 3507 (1997).
- [5] B. Dickens, E. Balizer, A. S. DeReggi and S. C. Roth, *J. Appl. Phys.* **64**, 5092 (1988).
- [6] J. C. Hicks and T. E. Jones, *Ferroelectrics* **32**, 119 (1981).
- [7] S. Ikeda, S. Kobayashi and Y. Wada, *J. Polym. Sci. Polym. Phys.* **23**, 1513 (1985).
- [8] A. K. Kulkarni, G. A. Rohrer, S. Narayan and L. D. Mcmillan, *Ferroelectrics* **116**, 95 (1991).
- [9] D. B. A. Rep and M. W. J. Prins, *J. Appl. Phys.* **85**, 7923 (1999).
- [10] A. Sheikholeslami and P. G. Gulak, *IEEE Trans. Ultrason. Ferroelectr. Freq. Control* **43**, 450 (1996).
- [11] A. Sheikholeslami and P. G. Gulak, *IEEE Trans. Ultrason. Ferroelectr. Freq. Control* **44**, 917 (1997).
- [12] D. E. Dunn, *IEEE Trans. Ultrason. Ferroelectr. Freq. Control* **41**, 360 (1994).
- [13] J.-H. Cho, H.-T. Chung and H.-G. Kim, *Ferroelectrics* **198**, 1 (1997).
- [14] C. B. Swayer and C. H. Tower, *Phys. Rev.* **35**, 269 (1930).
- [15] S. L. Miller, R. D. Nasby, J. R. Schwank, M. S. Rodgers and P. V. Dressendorfer, *J. Appl. Phys.* **68**, 6463 (1990).
- [16] S. L. Miller, J. R. Schwank, R. D. Nasby and M. S. Rodgers, *J. Appl. Phys.* **70**, 2849 (1991).
- [17] A. Vladimirescu, *The Spice book*. (Wiley, New York, 1994).
- [18] L. D. Landau and I. M. Khalatnikov, *Dok. Akad. Nauk SSSR.* **46**, 469 (1954).
- [19] S. Machlup and L. Onsager, *Phys. Rev.* **91**, 1505 (1953).
- [20] S. Machlup and L. Onsager, *Phys. Rev.* **91**, 1512 (1953).
- [21] Y. Makita, I. Seo and M. Sumita, *J. Phys. Soc. Japan.* **28**, Suppl. 268 (1970).
- [22] R. Seydel, *Practical Bifurcation and Stability Analysis. From Equilibrium to Chaos* Second Edition (Springer Interdisciplinary Applied Mathematics, 1994).
- [23] G. Bertotti, A. Magni, I. D. Matyergoyz, C. Serpico, *J. Appl. Phys.* **89**, 6710 (2001).
- [24] G. Gumbs and Mirsoslav, *J. Appl. Phys.* **73**, 5479 (1993).